Proceedings of the 26th International Conference on
Port and Ocean Engineering under Arctic Conditions
June 14-18, 2021, Moscow, Russia

Properties of drift ice and surface currents on Spitsbergen Bank

Marchenko, A.[1], Turnbull, I.[2], Kowalik, Z.[3], Marchenko, N.[1], Morozov, E.[4], Frey, D.[4]
[1] The University Centre in Svalbard, Longyearbyen, Norway
[2] Memorial University of Newfoundland, St. John's, Canada
[3] University of Alaska Fairbanks, Fairbanks, USA
[4] Shirshov Institute of Oceanology of RAS, Moscow, Russia

ABSTRACT

Results of field work performed on Spitsbergen Bank during 2017-2019 are discussed in this paper. Ice conditions on Spitsbergen Bank were analyzed using ice maps, drilling studies, and visual observations. The main findings of this research are the difference between measured ice drift velocities and water velocities calculated with the tide model in the shallow region of the bank with water depths of 25-35 m. The mean measured velocities exceeded the mean simulated velocities by 20%. The maximal measured velocities were greater than the maximal simulated velocities by 50%. Richardson numbers smaller 0.25 calculated from data recorded by Conductivity Temperature Depth (CTD) and Acoustic Doppler Current Profiler (ADCP) profiling indicated dynamic shear instability of the ocean current over the entire water column.

KEY WORDS: drift ice, ice edge, tide, boundary layer

INTRODUCTION

The shallow region of the Barents Sea with depths shallower than 100 m between Bear Island and Hopen Island is called Spitsbergen Bank (Fig. 1, left panel). High biological productivity (Henrich et al., 1997) supports the significant fishery activities on Spitsbergen Bank during the summertime (Gulliksen et al., 2009; ICES, 2019) which is performed mainly by fishing vessels with deadweights below 5000 GT (DNV GL, 2020). The inflow of Arctic water into the shallow Spitsbergen Bank causes a more extended ice season in this area compared with the other regions of the Barents Sea at similar latitudes. During the winter, ice cover combined with polar darkness stops plankton production, resulting in deficient food supply for benthic organisms. Therefore, winter fishing is performed at the periphery of Spitsbergen Bank around the Polar Front (DNV GL, 2020). Tankers and research vessels perform other shipping activities in the region. Sea ice and icebergs influence the shipping routes in winter; they are also a potential danger for the offshore activity to the southwest of Bear Island.

Cold water transported by the East Spitsbergen Current from the north interacts with warm

Atlantic water in the Barents Sea (Loeng, 1991). The boundary zone between these waters shown in Fig. 1 (left panel) by a double black line is called the Polar Front (Harris et al., 1998). The salinity and density of the Atlantic water is higher than the salinity and density of the Arctic water transported in the Barents Sea from the Arctic Ocean by the East Spitsbergen Current through the strait between North-East Land and Franz Josef Land. The temperature of "ideal" Arctic water is close to the freezing point (-1.9^{o}C), and salinity is below 34.5 PSU. The salinity of "Ideal" Atlantic water is around 35 PSU, and the temperature is above 0^{o}C (Oziel et al., 2015). Therefore, Atlantic water tends to occupy deeper ocean layers when it meets with colder and fresher Arctic water. One branch of Atlantic water penetrates in the Barents Sea through the Barents Opening, and the other branch follows the west coast of Spitsbergen and penetrates in the Barents Sea from the north between Svalbard and Franz Josef Land (Lind and Ingvalsen, 2012). Polar Front water is saltier than Arctic water but colder than Atlantic water (Fer and Drinkwater, 2014; Kedra et al., 2017). The shallow part of the Svalbard Bank to the north of Bear Island is occupied by well-mixed Svalbard Bank water with lower salinity than that of Polar Front water. Mixing is caused by strong tidal currents (Gjevik et al., 1994; Kowalik and Proshutinsky, 1995), wind forcing, and convection (Dobrovolsky, 1977; Fer and Drinkwater, 2014).

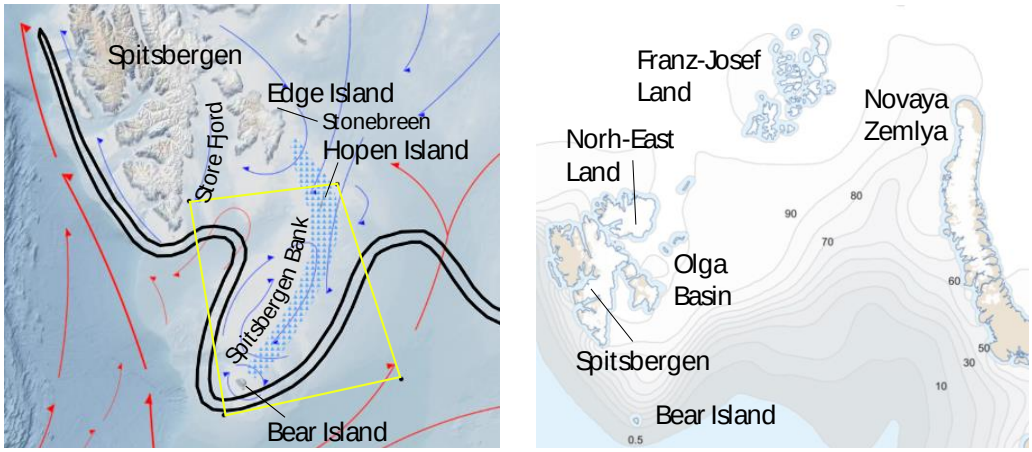

Figure 1. The study region in this paper. The black line shows the Polar Front between Arctic and Atlantic waters. Left: red and blue lines and arrows show directions of the currents of Atlantic and Arctic waters, cloud of blue triangles shows the Tidal Front (Fer and Drinkwater, 2014). The yellow square shows the area extending from 24^{o} to 16.5^{o}E, and 74^{o} and 77^{o}N. Right: Gray lines show isolines of ice concentrations in April over 1998-2017. (https://kart.barentswatch.no/?epslanguage=no).

Gjevik et al. (1990) discovered a substantial increase of tidal velocities on Spitsbergen Bank with a dominant M2 constituent and clockwise rotation. Principal axes of the M2 tidal ellipses extend from east-southeast to west-northwest, and the lengths of their major axes reach 1 m/s on the shallow Spitsbergen Bank and near Bear Island. The semidiurnal components S2 and N2 have nearly the same dynamic features as M2 with amphidromic points to the southeast from Hopen Island (Gjevik et al., 1994). Fer and Drinkwater (2014) specified the Tidal Front (Fig. 1, left panel) where the horizontal gradient of density, homogeneous in the water column, exceeded 0.01 kg/m^3 per km, dominated by negative salinity anomalies because of ice melt.

Numerical simulations of Gjevik et al. (1994) and Kowalik and Proshutinsky (1995) showed that clockwise eddies occur around Hopen Island, Spitsbergen Bank, and Bear Island under the influence of tides. The flow-through motion is realized around major bathymetric features and branches into flows interconnecting different regions. The speed of residual currents around

Bear Island and shallow Spitsbergen Bank changes in time with the spring-neap period, and the maximal speed is estimated to be on the order of 8 cm/s. The local eddies prevent residual flow-through and provide pathway routes for the exchange of water properties between various regions (Kowalik and Proshutinsky 1995). The diurnal tide resonates with shelf wave modes (Kasajima and Marchenko, 1991). Residual currents due to the diurnal tides occur at both the shallow areas and the shelf slope in the regions of maximum topographic slopes (Gjevik et al., 1994; Kowalik and Proshutinsky 1995).

Bear Island is located near the critical latitude of the M2 tide, 74.47^{o} N. Theoretical studies by Furevik and Foldvik (1996) demonstrated notable changes in the bottom boundary layer of the M2 tidal current at latitudes 72^{o} – 79^{o} N which can lead to the Kelvin–Helmholtz instability of shear flow in stratified fluid. Analysis of CTD data near the critical latitude for the M2 constituent in the eastern part of the Barents Sea indicates that the stability is closely linked to the velocity shear. Large vertical shear correlates with low stability and a lower shear with higher stability. Nevertheless, the observed values of the density gradient and the M2 tidal velocity shear yielded in the values of the Richardson numbers between 16 and 400 when fully developed turbulence does not exist. Furevik and Foldvik (1996) assumed that local values of the Richardson numbers could be higher comparing to the values estimated with vertically averaged and time-averaged density gradients.

In this paper, we describe the oceanographic and ice conditions on Spitsbergen Bank during the ice season based on analysis of ice maps and results of field work in April 2018 performed from the research vessel "Polarsyssel". The paper focuses on the investigation of the vertical structure and stability of the tidal current and on the influence of tidal current on sea ice drift in the shallow water region of the bank.

ICE CONDITIONS IN SPITSBERGEN BANK

Sea ice was observed and investigated during the research cruises of the Polarsyssel in the region of Spitsbergen Bank on April 22-30, 2017; April 24-30, 2018; and April 23-29, 2019. The investigations were performed in ice covered regions of the bank. Since Spitsbergen Bank is an open area of the Barents Sea, the ice conditions are very dynamic and weather-dependent. The extension of sea ice on Spitsbergen Bank on April 27, 2018, is shown in the left panel of Fig. 2. The ice map was taken from the web-based resource https://cryo.met.no. The ice tongue extending from Hopen Island to Bear Island is a typical feature of the ice cover on the bank. Right panels in Fig. 2 show the development of ice conditions on the bank over five days. A cyclonic ice gyre formed near the underwater hill where minimal water depth reaches 17 m according to the map onboard the Polarsyssel. The underwater hill is also known as Kelp forest place (Henrich et al, 1997).

The areas covered by sea ice are associated with water depths shallower than 100 m. Depending on the weather conditions, the ice edge may extend to Bear Island or be located north of the island. Winds from the north influence ice drift to Spitsbergen Bank from the Olga Basin. Winds from the south might displace sea ice from the bank to Store Fjord and Hopen Island. Winds from the west and east displace ice in the regions of warm Atlantic currents, where the oceanic heat flux to the ice bottom influences ice melt (Fig.1, left panel). Latitude 75^{o} N can be considered as a boundary characterizing the northern position of the ice edge on Spitsbergen Bank.

Drift ice observed on Spitsbergen Bank during the cruises consisted of consolidated sea ice floes with drafts up to 9 m and diameters of 20-50 m (Fig.3, right panel); there are relatively large areas with slushy ice, sea ice floes with thicknesses of 30-40 cm and diameters 10-100 m,

and bergy bits (Fig. 3, left panel) (Marchenko, 2019). Thick consolidated floes were found on each cruise, and their occurrences were not rare events. Nevertheless, their number was smaller than the number of floes with 30-40 cm thicknesses. Large areas of slushy ice were observed when the Polarsyssel approached shallow areas with depths smaller than 50 m.

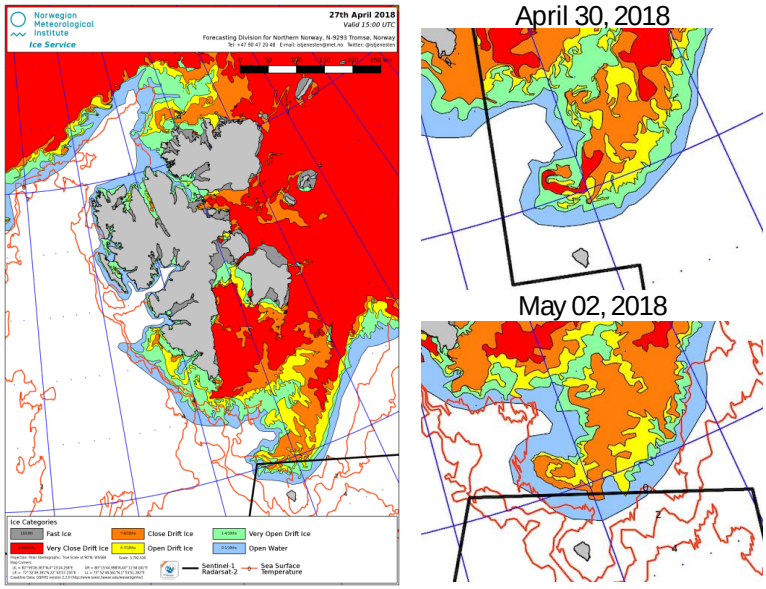

Figure 2. Development of ice conditions on Spitsbergen Bank from April 27 to May 02, 2018.

Laser scanning and drilling studies were performed to investigate the structure and shape of the thick floes (Marchenko and Marchenko, 2019). Analysis of thin sections taken from ice cores showed that the top layer of the floes has almost a granular structure with small elongations of grains in the vertical direction. In the middle layer, the thin sections showed a more columnar structure. Salinity (2-7 ppt) of ice cores taken from the floes showed that they consist of first-year sea ice. The shape analysis suggested that these floes were completely consolidated ice ridges. We did not observe strong interaction between floes of drifting ice on Spitsbergen Bank and we assume that the observed consolidated ice ridges were not of local origin. The motion of drifting ice on Spitsbergen Bank can be considered as free drift.

Figure 3. Drift ice and bergy bit (left), ice floe with maximum thickness of 6 m (right). Photographs taken from onboard the Polarsyssel on April 28, 2018.

The blue dots in the left panel of Fig. 4 show the days when the ice edge crossed the latitude 75° N to the north of Bear Island since 1998. The data were downloaded from https://cryo.met.no. This web-based resource does not provide ice maps in 2011, and the

lack of data for this year is shown by the solid white band in the left panel in Fig. 4. The first appearance of sea ice at 75° N after the summer seasons was registered at the end of December, and the last observations of ice appearance at 75o N were registered in June. Most frequently sea ice has been found at 75° N in March and April. The right panel in Fig. 4 shows the annual number of days (AD) when the ice edge crossed 75° N latitude to the north of Bear Island since 1998. The AD reached a maximum of 150 days in 2003 and it was equal to 138 in 2020. The minimums of AD reached two days in 2012, and five days in 1999. The mean value of AD shown by the solid black line in Fig. 4 is 60 days. The standard deviation of the AD represented by the difference between the dotted black lines and the solid mean black line is 36.6 days.

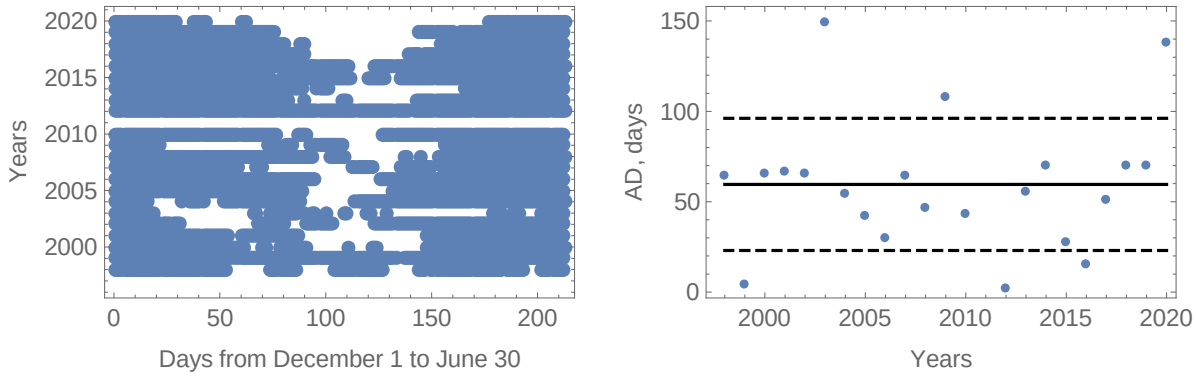

Figure 4. Occurrence of sea ice at 75° N latitude to the north of Bear Island since 1998. Left panel: days when sea ice was recorded at 75° N. Right panel: Annual number of days (AD) when sea ice was recorded at 75° N. Data for 2011 are absent.

FIELD WORKS IN APRIL 2018

The field measurements were performed on the drifting ice floe and onboard the Polarsyssel on April 27-28, 2018. The trajectory of the Polarsyssel (moored to the drifting ice floe) during the measurements is shown in the left panel of Fig. 5 by the blue line. The field work was performed in shallow water with depths smaller than 35 m near an underwater hill located to the north of Bear Island. The minimum depth in the region depicted on the navigational maps available on the bridge was 17 m. Seabed bathymetry in the area around the ship trajectory from 09:00 to 21:00 UTC, April 28, is shown in the right panel of Fig. 5. The numbers 1-7 show the ship's location at 09:30, 11:00, 13:00, 15:00, 17:00, 19:00 and 21:00 respectively.

An ice tracker (IT) (Oceanetic Measurements Ltd.) was deployed in the middle of the floe shown in the right panel of Fig. 3 on April 28. It transmitted Global Positioning System (GPS) coordinates with a 10-minute sampling interval by Iridium modem via satellite. Seawater temperature and salinity were recorded by the Conductivity Temperature Depth (CTD) meter SBE-19P over the water column (CTD profiling). The Acoustic Doppler Current Profiler (ADCP) Nortek AWAC 400 kHz was used to record water velocities. The ADCP was fixed on a wire extending from the shipboard to a depth of around 5.5 m and recorded water velocities with a sampling interval of 10 minutes and a spatial resolution of 1 m (cell size) over the water column from 6.5 m depth to the bottom.

RESULTS OF FIELD MEASUREMENTS

The trajectory of the IT recorded during April 28 to May 3 is shown by the black curve in the left panel of Fig. 5. The blue points in the left panel of Figure 6 show the East and North

components of the IT velocity calculated from the GPS data. The yellow points in the same figure show the components of depth averaged water velocity computed by the tide model TPXO (Egbert and Erofeeva, 2002) for the region and the time under consideration. The right panel of Fig. 6 shows the IT speed (blue curve) and simulated tidal current speed (yellow curve) versus time. It is obvious that the IT speeds are greater than the simulated tidal current speeds. The mean values of the IT speeds and simulated tidal current speeds were 0.83 m/s and 0.62 m/s, respectively, as shown by the blue and yellow lines in the right panel of Fig. 6.

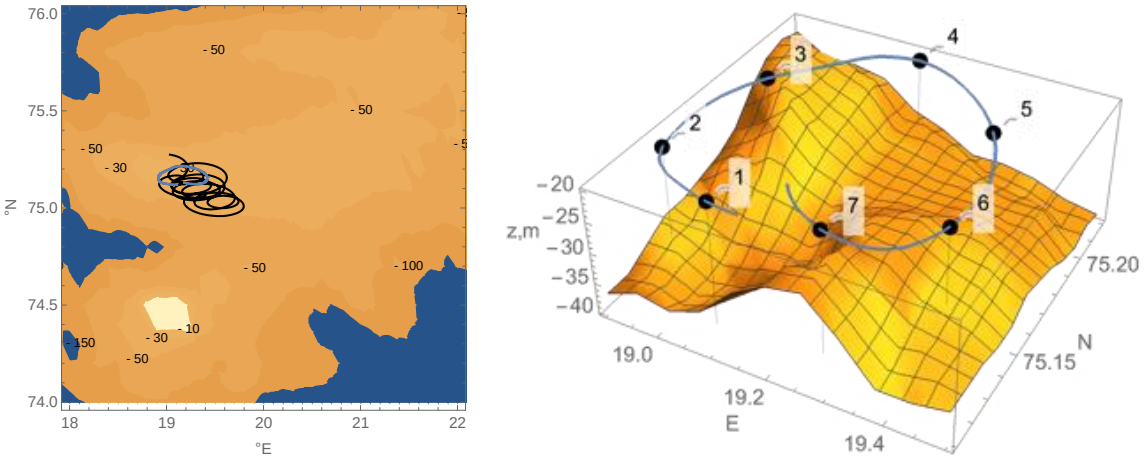

Figure 5. Bathymetry map near Bear Island and trajectories of the Polarsyssel (blue line) and the ice tracker (black line) in April 2018 (left). Trajectory of the Polarsyssel drift on 09:00-21:00 UTC, April 28, 2018, and seabed bathymetry (right).

Figure 7 shows wind speed and direction measured by a meteorological station on Bear Island. Wind speeds were mainly less than 6 m/s during April 28 - May 01 and increased up to 14 m/s on May 03. The wind direction changed from the north to the west, south and southeast and east directions during April 28 - May 01. Then, the wind turned back to the southeast direction during May 02-03. The right panel in Fig. 6 shows that fluctuations of IT speed increased during May 02-03 together with the increase in the wind speed. The wind action on ice was small in comparison to the water drag during April 28 - May 01.

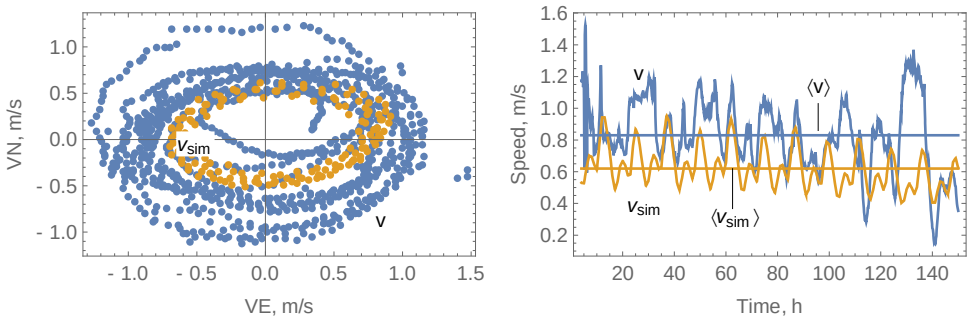

Figure 6. Components of IT velocities (blue points) and simulated tidal current velocities (yellow points) computed for a 150-hour time interval beginning from 15:00 UTC, April 28, 2018 (left). IT speeds (blue curve) and simulated tidal current speeds (yellow curve) versus time (right).

According to the data from CTD profiling, vertical profiles of the water density are well approximated by the formula $z = -5 - 200(\Delta\rho - 27.78)$, where z (m) is the vertical upward-directed coordinate, and $\Delta\rho = \rho_w - 1000$ (kg/m3) is the difference between sea

water density and 1000 kg/m3. The vertical gradient of sea water densities is estimated by the formula $\partial\rho_w/\partial z = -5\cdot 10^{-3}$ kg/m^4, and the squared Brunt-Väisälä frequency $N^2 = -g\rho_w^{-1}\partial\rho_w/\partial z$ equals $4.7\cdot 10^{-5}$ s^{-1} over the entire water column

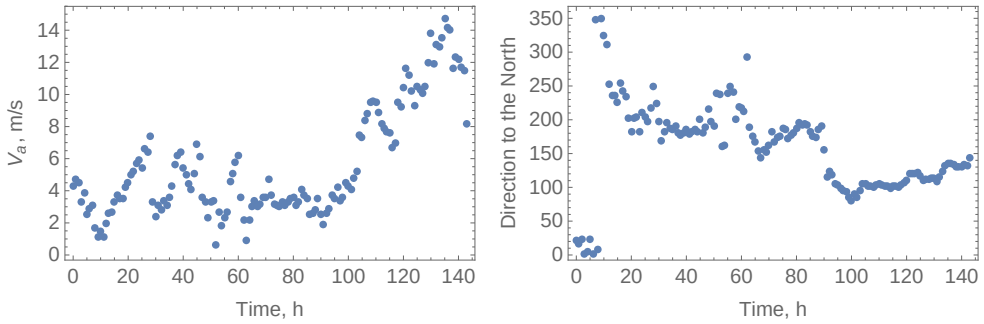

Figure 7. Wind speed (left) and direction (right) measured at Bear Island beginning from 00:00 UTC, April 28, 2018.

Vertical profiles of ocean current velocities were measured by the ADCP Nortek AWAC (400 kHz) deployed from the vessel in a downward-looking position. The bin size was 1 m, and the profile interval was 10 minutes. The ADCP was deployed at 5.5 m depth, and the first bin of the records corresponds to the depth interval from 6.5 m to 7.5 m. The first measurement started at 09:07 UTC, and the last measurement was at 20:57 UTC on April 28, 2018. The ADCP recorded current velocities relative to the ship velocity. Therefore, the ship velocity was added to ADCP velocities to calculate current velocities in the ground-based reference frame. The data were processed using the operation ListDensityPlot in Wolfram Mathematica software. The procedure Fit was used for the time-interpolation of the velocity components by third-order polynomials at each depth. This procedure reduced the noise level of the raw data.

Vertical profiles of current speed in the ground-based reference frame are shown in Fig. 8. The numbers show the time of measurement in hours since the first measurement at 09:07 UTC, April 28, 2018. One can see that the bottom boundary layer extended from the bottom to the first bin on the profiles recorded from t =1.0 h to 3.0 h. Maximal ocean current speeds in the range of 1.14-1.24 m/s were recorded at t =4.0 h at the shallowest point along the ship trajectory with a water depth of 25 m. The vertical gradient of current speed is not significant along this profile. This can be explained by the influence of Kelp forest on the boundary layer. Boundary layers extending from the seafloor to 10 m are visible on the profiles recorded from t =7.5 h to 10.0 h. Several profiles show an increase of current speed near the seabed.

The dependencies of the north and east velocity components in the ship-fixed reference frame are shown in Fig. 9 versus time. Vertical gradients of the velocities are clearly seen in the figure and are consistent with the structure of the first mode of internal waves in the fluid with constant stratification (Gerkema and Zimmerman, 2008). Since the velocities were measured in the moving reference frame their temporal variability can be related to topographic ocean currents. The magnitude of the vertical velocity gradient is designated with the formula $\Delta_z v = \sqrt{(\partial v_E/\partial z)^2 + (\partial v_N/\partial z)^2}$, where v_E and v_N are the east and the north components of current velocity. The Richardson number $Ri = N^2(\Delta_z v)^{-2}$ indicates dynamic instability of shear currents in stratified fluid when $Ri < 0.25$ leading to turbulence and water mixing (Taylor, 1931). Figure 10 shows the magnitudes of the vertical velocity gradients (left panel) and the Richardson numbers (right panel) calculated with $N^2 = 4.7\cdot 10^{-5}$s-1 versus time and water depth. It is obvious that $Ri < 0.25$ over almost the entire water column. This indicates dynamic shear instability of the water flow in the shallow region of Spitsbergen Bank.

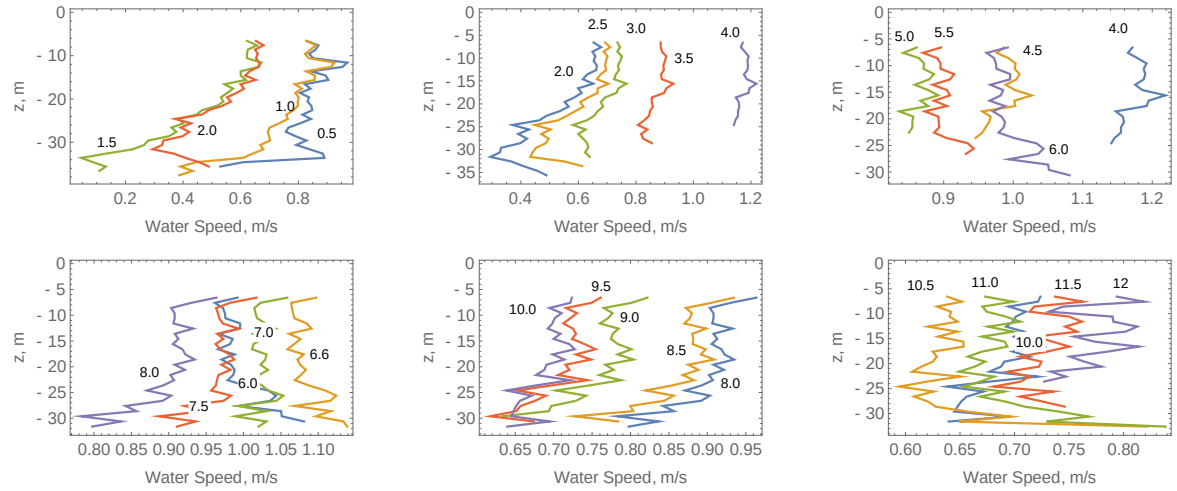

Figure 8. Vertical profiles of the horizontal current speeds measured by the ADCP. The first measurement was performed at 09:07:37 UTC, April 28, 2017. Numbers show the time (hours) after the first measurement.

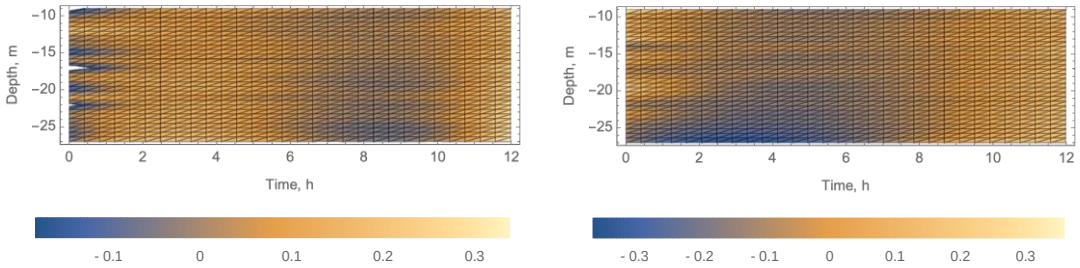

Figure 9. The zonal (left) and meridional (right) ADCP-recorded current velocities (m/s) from April 28 from 09:07 to 20:57, UTC, 2018.

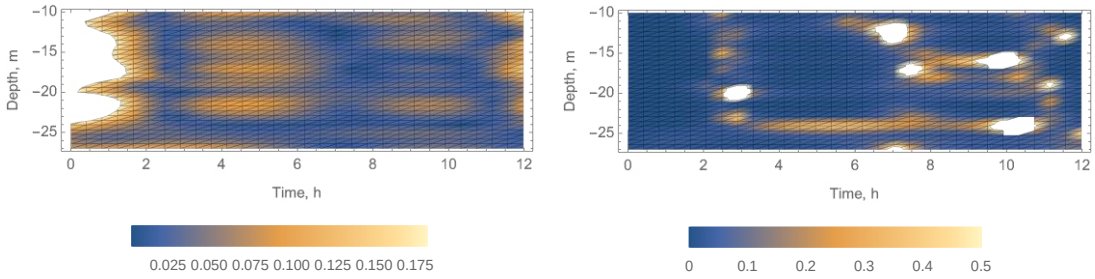

Figure 10. Magnitudes of vertical gradients of the horizontal ADCP-recorded current velocities (1/s) from April 28 from 09:07 to 20:57 (UTC), 2018 (left). The Richardson numbers calculated with the ADCP-recorded current velocities (right).

DISCUSSION AND CONCLUSIONS

Analysis of ice conditions showed that sea ice can be observed for a significant period every year on Spitsbergen Bank. A criterion for comparison is the annual number of days when ice was found at 75ºN latitude. Most frequently, sea ice was observed at 75º N in March and April. Since 1998, the annual number of days (AD) when sea ice was present at 75º N reached a maximum of 150 days in 2003 and was equal to 138 days in 2020. The minimum numbers of AD reached two days in 2012, and five days in 1999. The mean value of AD is 60, and the standard deviation is 36.6 days.

Despite the relatively stable location of sea ice on Spitsbergen Bank, the ice is transported by strong tidal currents. Measurements of the drifting ice floe velocity and current velocities were performed in the region with water depths of 25-35 m located to the north of Bear Island around 19.3°E and 75.1°N. The maximum speed of the ice tracker deployed on the floe reached 1.5 m/s, the minimum speed was 0.15 m/s, and the mean speed was 0.83 m/s. The ice tracker trajectories over one semidiurnal cycle were almost circular, and the ice tracker moved with clockwise rotation. This motion corresponds well to the characteristics of tidal currents on Spitsbergen Bank (Gjevik et al., 1994), but the mean speed of the tidal current calculated for the locations and times of the IT drift with the TPXO model was 0.62 m/s. Thus, the mean measured velocities exceeded the mean simulated tidal current velocities by 20%, and the maximum measured velocities exceeded the maximum simulated tidal current velocities by 50%.

We hypothesize that the boundary layer effect in the proximity of the M2 critical latitude 74.47^{o} N described by Furevik and Foldvik (1996) explains the difference. In shallow water the boundary layer can extend over the entire water column and cause significant differences between the mean current velocity averaged over the sea depth and the surface current velocity. The IT velocity was almost the same as the surface current velocity, while the tide model calculates current velocity averaged over the sea depth, and it leads to the differences. The Richardson numbers calculated from the measured current velocities were smaller than 0.25 over almost the entire water column in the shallow region with 25-35 m depths located to the north of Bear Island. This shows dynamic instability of the tidal currents on Spitsbergen Bank whose existence was discussed by Furevik and Foldvik (1996) and Rippeth et al. (2017). The dynamic instability influence water mixing and a reduction of ocean heat flux in shallow water regions of Spitsbergen Bank. It causes fast formation of ice in cold weather, and partially explain extended ice season in Spitsbergen Bank in comparison with other regions of the Barents Sea located at the same latitude.

ACKNOWLEDGEMENTS

The work was supported by the Research Council of Norway through the Centre for Sustainable Arctic Marine and Coastal Technology (SAMCoT) and IntPart project Arctic Offshore and Coastal Engineering in Changing Climate (AOCEC).

REFERENCES

BarentsWatch, 2020. "Map Service." from https://kart.barentswatch.no/?epslanguage=no.

DNV GL, 2020. "The Arctic risk map." from https://maps.dnvgl.com/arcticriskmap/.

Dobrovolsky, A.D., Ed., 1977. Convective Mixing in the Sea. Moscow: University Press, 239 pp.

Egbert, G.D., Erofeeva, S.Y., 2002. Efficient inverse modelling of barotropic ocean tides. *J. Atmos. Oceanic Technol*., 19(2), 183-204.

Fer, I., Drinkwater, K., 2014. Mixing in the Barents Sea Polar Front near Hopen in spring. J. *of Marine Systems*, 130, 206-218.

Furevik, T., Foldvik, A., 1996. Stability at M2 critical latitude in the Barents Sea. *J. Geoph. Res*., Vol. 101, NC4, 8823-8837.

Gerkema, T., Zimmerman, J.T.F., 2008. An introduction to internal waves. Lecture Notes, R. Neth. Inst. for Sea Res., Den Burg, 207 pp.

Gjevik, B., Nost, E., Straume, T., 1990. Atlas of tides on the shelves of the Norwegian and the Barents Seas. Rep. F&U-ST 90012, Dept. of Math., Univ. of Oslo, report to Statoil, Stavanger.

Gjevik, B., Nost, E., Straume, T., 1994. Model simulations of the tides in the Barents Sea. *J. Geoph. Res.*, Vol. 99, NC2, 3337-3350.

Gulliksen B, Hop H, Nielssen, M., 2009. Benthic life. Ch 15. In: Sakshaug E, Johnsen G, Kovacs K (eds) Ecosystem Barents Sea.Tapir Academic Press, Trondheim.

Harris, C.L., Plueddemann, A.J., Gawarkiewicz, G.G., 1998. Water mass distribution and polar front structure in the western Barents Sea. *J. Geoph. Res*., 103, NO. C2, 2905-2917.

Henrich, R., Freiwald, A., Bickert, T., Schafer, P., 1997. Evolution of an Arctic open-shelf carbonate platform, Spitsbergen Bank (Barents Sea). In: James NP, Clarke JAD (eds) Cool-water carbonates. SEPM Spec Pub No 56: 163–181.

ICES. 2019. Barents Sea Ecoregion – Ecosystem overview. In Report of the ICES Advisory Committee, 2019. ICES Advice 2019, Section 5.1. 12 pp.

Kasajima Y., Marchenko A., 2001. On the excitation of resonant double Kelvin waves in the Barents Sea Opening. *Polar Research*, 20(2): 241-248.

Kedra, M., Renaud, P.E., Andrade, H., Goszczko, I., Ambrose WG Jr., 2013. Benthic community structure, diversity, and productivity in the shallow Barents Sea bank (Svalbard Bank). *Marine Biology*, 160, 805–819.

Kowalik, Z., Proshutinsky, A. Yu., 1995. Topographic enhancement of tidal motion in the western Barents Sea. *J. Geoph. Res*., Vol. 100, NC2, 2613-2637.

Lind, S., Ingvaldsen, R.B., 2012. Variability and impacts of Atlantic Water entering the Barents Sea from the north. *Deep-Sea Research* I, 62, 70-88.

Lind, S., Ingvaldsen, R.B., Furevik, T., 2018. Arctic warming hotspot in the northern Barents Sea linked to declining sea-ice import. *Nature Climate Change*, 8, 634-639.

Loeng, H., 1991. Features of the physical oceanographic conditions of the Barents Sea, *Polar Research*, 10, 1, 5-18.

Marchenko, N., 2019. Ice at its southern limit in the Barents Sea: field investigation near Bear Island in April 2017-2018. *POAC19-58*.

Marchenko, A., Marchenko, N., 2019. Characteristics of ice drift and waves on Spitsbergen-banken. *POAC-33*.

Nost, E., 1994. Calculating tidal current profiles from vertically integrated models near the critical latitude in the Barents Sea. *J. Geop. Res*., Vol. 99, NO. C4, 7885-7901.

Oziel, L., Sirven, J., Gascard, J.-C., 2015. The Barents Sea polar front and water masses variability (1980–2011). *Ocean Sci. Discuss*., 12, 449–492.

Rippeth, T. P., Vlasenko, V., Stashchuk, N., Scannell, B. D., Green, J. A. M., Lincoln, B. J., Bacon, S., 2017. Tidal conversion and mixing poleward of the critical latitude (an Arctic case study). Geophysical Research Letters, 44, 12,349–12,357.

Taylor, G.I., Effect of variation in density on the stability of superposed streams of fluid, *Proc. R . Soc. London A*, 132,4 99-523, 1931.